

ARTICLES

Advanced Continuum Approaches for Treating Time Correlation Functions. The Role of Solute Shape and Solvent StructureDrew F. Parsons,[†] Mikhail V. Vener, and Mikhail V. Basilevsky**Karpov Institute of Physical Chemistry, ul. Vorontsovo Pole 10, Moscow 103064, Russia**Received: July 2, 1998; In Final Form: December 14, 1998*

Time correlation functions describing the solvent relaxation around a molecule of coumarin-153 and a benzophenone anion in acetonitrile are calculated using dynamical continuum theories of solvation with an experimental dielectric function $\epsilon(\omega)$ including the resonance absorption region of the solvent. Apart from the local model with a single molecular-shaped solute cavity of the solute studied previously, a new dynamic local model with a double molecular-shaped cavity and a dynamic nonlocal theory with a spherical cavity are presented, both of which introduce elements of solvent structure. It is shown that both local models, one- and two-cavity, exhibit experimentally unobserved oscillations in the shorter time region $t < 1$ ps, although the experimental asymptote for $t > 1$ ps for coumarin is obtained. The dynamics of the two-cavity model are not seen to differ from those of the one-cavity model. The nonlocal dynamic theory is shown to be able to suppress these oscillations, but the long-time asymptote differs markedly from that of the local theories. The nature of this asymptote is studied analytically.

1. Introduction

It was shown in recent theoretical papers^{1–3} that an advanced continuum approach may be successfully used for studying time-dependent solvation phenomena. The key step in all continuum treatments is to use the complex-valued solvent dielectric function $\epsilon(\omega)$, a function of the angular frequency ω , as a phenomenological characteristic of solvent dynamics.^{4,5} The corresponding dynamical equations prove to be a generalization of the static equilibrium equations of continuum solvation theory, with the simple substitution $\epsilon_0 \rightarrow \epsilon(\omega)$, where ϵ_0 is the static dielectric constant. Therefore, advanced approaches can be classified by the level of sophistication used in their static counterparts. In comparison to the earlier Born-like static solvation models with spherical solute cavities,^{5,6} one may improve the theory by, first, considering cavities with a real molecular shape and, second, by making allowance for spatial dispersion effects, bringing elements of the solvent molecular structure into continuum theory. The former (cavity shape) effect was first studied with ellipsoid-shaped cavities^{1,7} and the treatment was extended recently for cavities of arbitrary shape.^{2,3} The second (solvent molecular structure) effect was discussed within the MSA^{8–10} and other^{11,12} models and also by a phenomenological nonlocal approach.¹³ Each of these treatments used simple spherical approximations. Earlier studies were mainly focused on the asymptotic long-time behavior of time correlation functions (TCFs) and average decay characteristics extracted from measurements of time-dependent solvent Stokes shifts.^{6,7,11,12,14} The complete time domain of experimentally

available TCF kinetic curves also includes short and intermediate time regions ($10 \text{ fs} < t < 1 \text{ ps}$) for which, in theoretical calculations, an accurate description of the dielectric function in intermediate- and high-frequency regions ($10^{12} < \omega < 10^{14} \text{ rad s}^{-1}$) is required. As shown recently,^{1,3,5,15} the most effective way of incorporating the dielectric function in this, the so-called resonance or far-infrared region (FIR),¹⁶ is by performing straightforward numerical calculations using experimentally measured data for $\epsilon(\omega)$.

The objective of the present work is to study systematically the relative importance of the different ingredients in the advanced continuum theories as they attempt to describe the time dependence of solvent Stokes shifts. We consider separately the role of the solute cavity shape and solvent molecular structure effects. The first effect of cavity shape is studied in terms of two modern advanced local theories. The simpler of these has been considered previously^{2,3} and places the solute in a single cavity surrounding the solvent. The other local theory attempts to model elements of solvent structure by placing the solute within two surrounding cavities¹⁷ (more details below); the layer between these cavities is said to correspond to the first solvation shell.

The second effect due to solvent structure is developed from a recent nonlocal electrostatic model, explicitly accounting for the excluded volume of a solute.^{18,19} In the simplest version of a spherical cavity, this second effect due to solvent molecular structure is governed by the dimensionless parameter λ/a , a ratio of the average size of the solvent (correlation length λ) and solute (cavity radius a) particles. The local models correspond to the limiting case $\lambda/a \rightarrow 0$, and we obtain a hierarchy of models: one-cavity local model \rightarrow two-cavity local model \rightarrow nonlocal model.

* E-mail: basil@cc.nifhi.ac.ru.

[†] Laboratoire de Chimie Théorique, Université de Nancy I, B.P. 239, 54506 Vandœuvre-Nancy, France.

The whole range of TCF time evolution is covered by using an accurate numerical representation of an experimental dielectric function in the resonance frequency region. By combining these techniques, a reliable conclusion concerning the general validity of continuum solvation models becomes available. We shall learn that the double-cavity local model, developed for calculating static nonequilibrium solvent effects,¹⁷ does not provide any dynamical effects differing from the simpler one-cavity model. The nonlocal dynamical theory will, however, be seen to be capable of reducing oscillations, which are found in the short-time kinetics of local calculations³ but not observed in experiments; however, the model seems to predict a longer time scale than that suggested by local calculations.

2. Methodology of Calculations

2.1. The Born–Kirkwood–Onsager (BKO) Model. This method of computing static solvation effects is commonly applied.²⁰ According to this model, the cavity for the solute is constructed as a union of interlocking spheres, each centered on an atom of the solute molecule. It is also known as the polarizable continuum model (PCM).²⁰

The linear response approach relates the solute charge distribution ρ to the response field Φ via the expression

$$\Phi = \hat{K}\rho \quad (2.1)$$

where \hat{K} is a linear integral operator. In general, it is a nonlocal operator. Typically, an explicit representation of \hat{K} is in practice unavailable; an approximation to it is provided by calculating a matrix representation defined on some limited basis of charge distributions ρ_{ab} (use of the double index is seen to be appropriate when a CI treatment of the solute electronic structure is invoked). The definition for this matrix, known as the reorganization matrix,

$$\begin{aligned} T_{ab,cd}(0) &= \int d^3r \rho_{ab} \Phi_{cd} \\ &= \int d^3r \rho_{ab} \hat{K} \rho_{cd} \end{aligned} \quad (2.2)$$

is taken from ref 2, with the sign given opposite to that of earlier publications.^{21,22} Within the BKO (or PCM) model the response field is given by

$$\Phi(r) = \int_S d^2r' \frac{\sigma(r')}{|r - r'|} \quad (2.3)$$

(the integral being taken over the cavity surface S), where σ is the surface charge density induced by the solute charge ρ . It is determined by solving the following linear integral equation involving ρ :

$$\sigma(r) = \frac{1}{4\pi} \left(1 - \frac{1}{\epsilon_0}\right) \{[\hat{V}\rho](r) + [(\hat{S} + 2\pi)\sigma](r)\} \quad (2.4)$$

where $r \in S$. Operators \hat{V} and \hat{S} are defined explicitly in the Appendix (here $\hat{S} \equiv \hat{S}_{11}$ in eq A.2).

As shown in ref 2, to calculate the ω -spectrum of the solvation energy, we need to determine the elements of the reorganization matrix $T(\omega)$, which can be derived in the same way as the elements of the static matrix $T(0)$ in eq 2.2, replacing the response field Φ with the complex quantity $\Phi(\omega)$, calculated from eq 2.3 using $\sigma(\omega)$ instead of σ . The complex quantity $\sigma(\omega)$ is calculated by replacing the dielectric constant ϵ_0 with the dielectric function $\epsilon(\omega)$ in the BKO integral equation defining σ . When the resulting complex equation is separated

into two parts, two equations are obtained in two unknown functions, the real and imaginary parts of the total complex surface charge density. It should be noted that the method developed in ref 3 is completely equivalent to the time-dependent BKO calculation, although its technical implementation looks quite different.

2.2. Frequency-Resolved Cavity Model (FRCM). The FRCM model¹⁷ is similar to the BKO model but differs by separating the inertialless (high-frequency) response of the medium from the inertial (low-frequency) one. The solute is surrounded by two surfaces S_1 and S_2 , each of which is constructed as a collection of spheres similar to the BKO model. For the first cavity, contained within the internal surface S_1 , the radii of the spheres are defined as $r_1 = \kappa r_{vdW}$, where $\kappa = 0.9$ is a universal empirical factor, common for all solvents. Here r_{vdW} is the van der Waals radius of the particular atom. The radii r_2 defining the external surface S_2 are given by

$$r_2 = r_1 + \delta = 0.9r_{vdW} + \delta \quad (2.5)$$

where δ is another empirical constant, pertaining to the given solvent (it correlates with the characteristic size of a solvent molecule). Between the two surfaces the medium is modeled by the inertialless high-frequency dielectric constant ϵ_∞ , outside of the outer cavity the medium is modeled by the static dielectric constant ϵ_0 . This layer between the surfaces corresponds to the first solvation shell. The FRCM scheme allows consistent calculations of both equilibrium and nonequilibrium effects,²³ which is impossible with the less flexible BKO scheme.²⁴ Calculation of the electric field in this scheme amounts to simultaneously solving two equations describing the surface charge densities on the two cavities, namely σ_∞ (on the inner surface) and σ (on the outer).

In this paper, for the sake of simplicity in calculating solvation dynamics, we apply to the FRCM model the assumption that the charge density on the outer surface is sufficiently small for its influence on the inner charge density to be neglected.¹⁷ This simplification would appear to be justified since the static ($\omega = 0$) solvation energies calculated in this way agree sufficiently well (to within about 15%) with the exact static FRCM values. Using this approximation, the first equation, describing σ_∞ , may be separated from the second. It is then identical to the ordinary BKO equation with dielectric constant ϵ_∞ and so is solved using the BKO method mentioned above. σ_∞ then enters as a parameter into the second equation describing σ , which effectively becomes a BKO equation with scaled parameters. Similarly to the BKO case described above, calculations of dynamics are performed by replacing ϵ_0 with the complex number $\epsilon(\omega)$, thereby the equation in σ splits into two equations describing the real and imaginary parts of σ (see Appendix). Solving these equations proceeds in a similar way as for the BKO case.

2.3. Algorithm for Calculating the Response Function $E(\omega)$ for Local Theories. The quantity we calculate is the inertial part $T_{in}(\omega)$ of the reorganization matrix $T(\omega)$ described in section 2.1 above. That is, $T_{in}(\omega) = T(\omega) - T(\omega = \infty)$. For the purposes of this paper we consider T_{in} to be a 2×2 matrix based on the two charge distributions corresponding to the ground and first excited electronic states, $\rho_{11} \equiv \rho_1$ and $\rho_{22} \equiv \rho_2$. More complicated approaches will include other charge distributions in the basis set using a configuration interaction ideology, the simplest case being a 3×3 matrix where the third charge distribution is given by the transition charge density ρ_{12} , but this will not be required here. For each charge distribution ρ_i we compute the corresponding polarization surface density σ_i

$= \sigma[\rho_i]$, for which the polarization potential is (see eq 2.3)

$$\Phi_i(r) = \int_S d^2r' \frac{\sigma_i(r')}{|r - r'|} \quad (2.6)$$

Note that since we are calculating the inertial reorganization matrix here, we do not include the inertialless polarization σ_∞ of the inner surface of the FRCM theory and it is to be understood that in eq 2.6 we are referring to $S = S_2$. This is the FRCM counterpart of the BKO expression (2.3). We are thus able to define the matrix $T(\omega)$ with elements (cf. eq 2.2)

$$T_{ij} = \int \Phi_i \rho_j d^3r \quad i, j = 1, 2 \quad (2.7)$$

from which we deduce the inertial matrix by subtracting the inertialless limit:

$$T_{in,ij}(\omega) = T_{ij}(\omega) - T_{ij}(\omega = \infty) \quad (2.8)$$

For coumarin-153 we then define the complex energy $E(\omega) = E_1(\omega) + iE_2(\omega)$ to be the reorganization energy $U_r(\omega)$

$$E(\omega) = U_r(\omega) = -\frac{1}{2}(T_{in,11}(\omega) + T_{in,22}(\omega) - T_{in,12}(\omega) - T_{in,21}(\omega)) \quad (2.9)$$

This quantity can be considered as a solvation energy for the charge distribution difference $\rho_2 - \rho_1$.

For benzophenone we define $E(\omega)$ to be the inertial part of the conventional ground-state solvation energy $U_s(\omega)$:

$$E(\omega) = U_{s,in}(\omega) = \frac{1}{2}T_{in,11}(\omega) \quad (2.10)$$

$E(\omega)$ measures the linear response of the solvent to the charge density ρ and henceforth will be called the "response function".

The TCF $C(t)$ is expressed in terms of $E(t)$, the inverse Fourier transform of $E(\omega)$; this expression can be reduced to a formula depending on the real part $E_1(\omega)^2$:

$$C(t) = 1 - \frac{2}{\pi} \int_0^\infty d\omega \frac{E_1(\omega)}{\Delta} \frac{\sin \omega t}{\omega} \quad (2.11)$$

where Δ is the energy change $E(\omega = 0) - E(\omega = \infty)$. A similar expression depending on the imaginary part $E_2(\omega)$ also exists (see Appendix A in ref 2), but eq 2.11 is more convenient in practical numerical calculations since the real part $E_1(\omega)$ attains its limits at high and low frequencies more quickly and so is more reliable.

2.4. Nonlocal Theory. A nonlocal continuum theory has been developed for practical calculations under the assumption of a simple spherical ion, based on a simple analytical formula for the solvation energy.¹⁹ A dynamical nonlocal calculation is performed in this paper by making the substitution $\epsilon(k) \rightarrow \epsilon(k, \omega)$ in this formula (see below). Let us write the simple dynamical function $\epsilon(\omega)$ (without spatial dispersion) and the static nonlocal dielectric function $\epsilon(k)$ in the form

$$\epsilon(\omega) = \epsilon + (\epsilon_0 - \epsilon)\Delta_\omega(\omega) \quad (2.12)$$

$$\epsilon(k) = \epsilon_\infty + (\epsilon_0 - \epsilon_\infty)\Delta_k(k) \quad (2.13)$$

Then a simple approximation to the full dielectric function $\epsilon(k, \omega)$ with both spatial and frequency dispersion may be given by multiplying together the inertial parts of the functions $\epsilon(\omega)$ and $\epsilon(k)$:

$$\epsilon(k, \omega) = \epsilon_\infty + (\epsilon_0 - \epsilon)\Delta_\omega(\omega)\Delta_k(k) \quad (2.14)$$

Note that eq 2.14 may be written as

$$\epsilon(k, \omega) = \epsilon_\infty + (\epsilon(\omega) - \epsilon_\infty)\Delta_k(k) \quad (2.15)$$

and so we see once again that the dynamical calculation may be considered as a simple substitution of $\epsilon(\omega)$ for the dielectric constant ϵ_0 in the static calculation. In writing $\epsilon(k, \omega)$ in this way, we neglect any k dependence that could be assigned within $\Delta_\omega(\omega)$; incorporating them at the present time would make the nonlocal problem intractable. We are, however, able to incorporate additional ω dependence into $\Delta_k(k)$, as will be described later, and so we have $\Delta_k(k) \rightarrow \Delta_k(k, \omega)$, which makes the approach suggested by eq 2.14 quite universal.

We accept a one-mode Lorentzian model for spatial dispersion, for which an analytical expression for the solvation energy is available.¹⁹ Although modern molecular dynamics simulations have demonstrated the existence of poles in $\epsilon(k)$, corresponding to oscillations in real space, it has been shown that their role is suppressed by fluctuations in the cavity size.²⁵ A nonlocal continuum theory has been developed that includes this effect, ultimately obtaining a monotonic solvation energy as a function of cavity radius. However, since this same result is obtained more simply with the Lorentzian model, we will assume here that the latter effectively incorporates the combined effect of cavity fluctuations and poles in the dielectric function and may be employed for an empirical study of solvation effects. Spatial dispersion is therefore given by

$$\Delta_k(k) = \frac{1}{1 + k^2\lambda^2} \quad (2.16)$$

We obtain the response function $E(\omega)$ by substituting $\epsilon(\omega)$ for ϵ_0 , as already mentioned; also we may permit the correlation length λ to change, falling to zero at the high frequencies characteristic of ϵ_∞ , writing $\lambda(\omega)$. We calibrate the cavity radius a_0 so as to reproduce the solvation (or reorganization) energy given by local calculations with a molecular-shaped cavity at the static ($\omega = 0$) limit. The high-frequency nonlocal solvation energy calculated using this radius is given by a Born-like formula when we assume $\lambda(\omega = \infty) = 0$

$$U_\infty = -\left(1 - \frac{1}{\epsilon_\infty}\right) \frac{Q^2}{2a_0} \quad (2.17)$$

and will in general differ from that given by the local theories (with a molecular-shaped cavity). $E(\omega)$ is given as the inertial part of the nonlocal solvation energy,¹⁹ after removing the inertialless part U_∞ :

$$E(\omega) = -\frac{Q^2}{2a} \left(\frac{1}{\epsilon_\infty} - \frac{1}{\epsilon(\omega)} \right) \times \frac{1 + \sqrt{\epsilon(\omega)/\epsilon_\infty}(\coth(a/\lambda(\omega)) - \lambda(\omega)/a)}{1 + \sqrt{\epsilon(\omega)/\epsilon_\infty}(\coth(a/\lambda(\omega)) - \lambda(\omega)/a) + \lambda(\omega)/a\sqrt{\epsilon_\infty/\epsilon(\omega)}} \quad (2.18)$$

We make special note of the ratio λ/a in this expression (for $\omega = 0$). This ratio, comparing the average size of the solvent particles to the solute, may be considered a measure of the degree of nonlocality of the system. The local limit is obtained when $\lambda/a \rightarrow 0$. More attention will be paid to this ratio in the Discussion.

3. Parametrization of the Dielectric Function

3.1. Definition of $\epsilon(\omega)$. We make use of an experimentally determined⁵ complex dielectric function $\epsilon(\omega)$ for acetonitrile.

Lower frequency microwave data were modeled by a single Debye function⁵ with parameters $\epsilon_0 = 35.8$, $\epsilon_\infty^{(MW)} = 3.51$, and $\tau_D = 3.37$ ps. The corresponding Debye peak in the absorption spectrum (imaginary part) lies at 1.5 cm^{-1} . A resonance peak in the absorption spectrum of acetonitrile at higher (FIR) frequencies and located approximately at 69 cm^{-1} had been used by Maroncelli by subtracting extrapolated microwave data²⁶ from experimental FIR data.²⁷ The corresponding real part of the resonance peak was calculated numerically using the Kramers–Kronig relations. Thus the full dielectric function $\epsilon(\omega)$ was obtained by adding the microwave Debye function to the FIR resonance data, yielding a static dielectric value of $\epsilon(\omega = 0) = 35.9$ and a high-frequency constant of $\epsilon_\infty = 1.80$, in agreement with the usual estimate of n_D^2 (for acetonitrile,⁵ $n_D = 1.34$).

As was mentioned above, there is no generally accepted formula for fitting the experimental data for dielectric dispersion in the resonance region. In most of the calculations presented here we use the original numerical data for the resonance peak of $\epsilon(\omega)$, as was similarly done in refs 1, 3, and 28. We also attempted approximating the $\epsilon(\omega)$ in this region using several analytical functions, the ideas of which were described in ref 29 (see discussion in section 5).

3.2. Definition of $\lambda(\omega)$. We accept a value of $\lambda = 6.68 \text{ \AA}$ for the correlation length for acetonitrile, calibrated using experimental solvation energies as in ref 19. In the local BKO and FRCM theories the parameters relating to the size of the solute, i.e., the cavity size and, in the FRCM theory, the distance δ between the two surfaces, do not change with frequency. The corresponding situation in the nonlocal theory is when the solvent correlation length $\lambda(\omega)$ remains constant: $\lambda(\omega) = \lambda$. However, it is more realistic to expect that there is no spatial dispersion at high frequencies. A simple model¹³ allows $\lambda(\omega)$ to fall monotonically from the static value of λ to zero:

$$\lambda(\omega) = \frac{\lambda}{1 + \omega^2 \tau_\lambda^2} \quad (3.1)$$

where $1/\tau_\lambda$ characterizes the center of the frequency region in which $\lambda(\omega)$ undergoes the transition from λ to 0. Following the methodology of ref 13, we gauge the value of τ_λ relative to the longitudinal time constant $\tau_L = \tau_D \epsilon_\infty / \epsilon_0$. For acetonitrile, $\tau_L = 0.169$ ps. The corresponding frequency $1/\tau_L$ is 5.91 cm^{-1} , lying between the Debye and resonance peaks of $\epsilon(\omega)$. The values of τ_λ which we will consider are $\tau_\lambda = \tau_L$, $\tau_L/2$, and $\tau_L/4$ as well as the limiting case of constant λ , $\tau_\lambda = 0$.

4. Results

The response function $E(\omega)$ was calculated as outlined above, and the desired TCF function numerically computed using eq 2.11. In contrast to our previous paper² we consider here only the time-domain representation of the computed kinetics, since, as mentioned above, there are no general formulas available for comparison that may fit the calculated values of $E(\omega)$ in the resonance region. Cole–Cole or Davidson–Cole models of dielectric dispersion are usually presented as functions in the frequency domain but seem to be available only for the orientational region ($\omega < 10^{12} \text{ rad s}^{-1}$, $t > 1$ ps).

4.1. TCF of Coumarin-153 in Acetonitrile. (BKO and FRCM Treatments.) The gas-phase geometry of coumarin-153 in the ground electronic state was found by standard optimization procedures using the PM3 method. The geometry of C-153 in the first excited singlet state was taken to be the same as that of the unexcited molecule. The value of the dipole

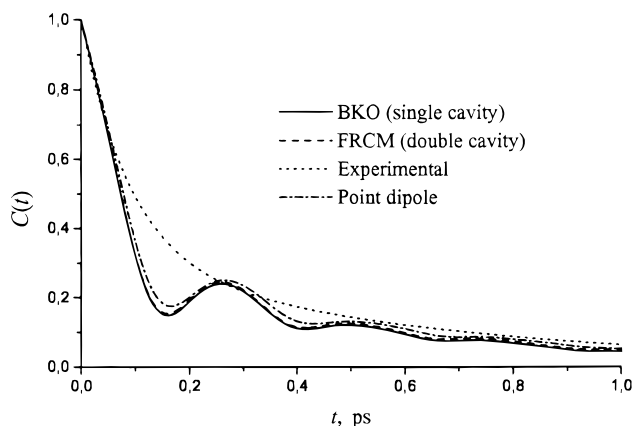


Figure 1. Time correlation functions $C(t)$ for coumarin-153 in acetonitrile. The calculated curves from both one-cavity (BKO) and two-cavity (FRCM) local theories are compared with the experimental curve. $C(t)$ for a point dipole in a spherical cavity is also given for comparison.

moment was equal to 5.8 D, compatible with the experimental³⁰ value 6.55 D. The $S_0 \rightarrow S_1$ transition causes a charge displacement from the amino group to the coumarin ring system, resulting in an S_1 dipole moment 13 D (PM3/CI calculations), in accord with experimental³¹ and AM1/CI^{5,32} data. The distance between inner and outer spheres in the FRCM model was set at $\delta = 2.2 \text{ \AA}$ so as to reproduce the reorganization energy $U_r = 0.17 \text{ eV}$ given by an exact static FRCM calculation (where $\delta = 1.8 \text{ \AA}$ ²³).

The calculated TCF functions are compared with available experimental data in Figure 1. It is noteworthy that the BKO (one-cavity) and FRCM (two-cavity) time correlation functions are essentially identical, even though the absolute values of the static reorganization energies differ greatly (BKO, 0.49 eV; FRCM, 0.17 eV). The TCF for a point dipole in a spherical cavity of radius a is also shown in Figure 1 for comparison and is seen to be close to the other calculated curves. The formula is

$$E(\omega) = -\frac{\epsilon(\omega) - 1}{2\epsilon(\omega) + 1} \frac{(\Delta\mu)^2}{a^3} \quad (4.1)$$

where $\Delta\mu = 7.2 \text{ D}$, the difference between the dipole moments in the ground and first excited states of coumarin-153, and $a = 4.2 \text{ \AA}$, the spherical radius giving the same cavity volume for coumarin-153 as that from the BKO calculations. These two parameters are not in fact essential since they are canceled out in $C(t)$. We note that the short-time decay may be approximately described with a Gaussian function.^{5,33} Contrary to experiment, both approaches show damped oscillation in the region varying from 0.1 to 1 ps. Comparison of the obtained TCFs with the curves computed in previous papers for C-153 in acetonitrile, see Figure 21 in Ref 5 and Figure 4 in ref 3 enables us to come to the following conclusions (as mentioned above, the calculations of ref 3 are at a theoretical level almost identical to our BKO calculations, the only difference being in the parametrizations):

1. Different methods of theoretical simulations^{3,5} of the short-time and long-time (asymptotic) decay provide a similar behavior in the TCFs.

2. Oscillations in the region from 0.1 to 1 ps appeared in all calculations that explicitly took into account the resonance absorption region in $\epsilon(\omega)$.

The fact that the second effect is observed in all theoretical treatments incorporating resonance may suggest that the local

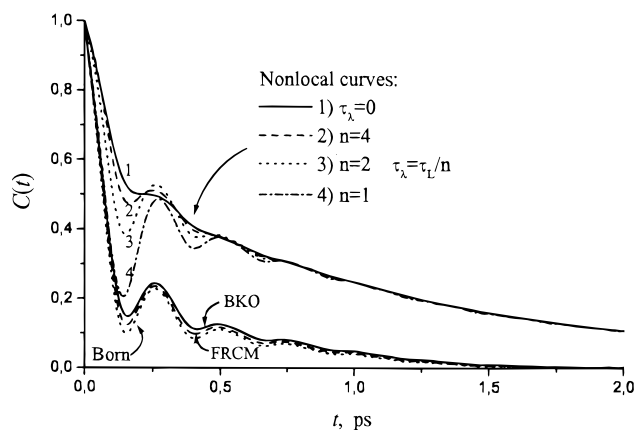


Figure 2. Time correlation functions $C(t)$ for a benzophenone anion in acetonitrile. The calculated curves from both one-cavity (BKO) and two-cavity (FRCM) local theories are compared with calculations from nonlocal theory ($\lambda = 6.68 \text{ \AA}$, $a = 2.35 \text{ \AA}$) for various values of the nonlocal transition time τ_λ (see section 3.2). The curve resulting from the Born solvation energy for a point charge in a spherical cavity is also given for comparison.

theories used in these studies are not altogether adequate for working in the resonance (and therefore short- and intermediate-time) region.

4.2. TCF of a Benzophenone Anion in Acetonitrile. The geometry of an benzophenone anion was taken to be the same as that of the neutral molecule found by standard optimization procedures using the PM3 method. The value of the dihedral angle between the planes of benzene rings was taken to be 30° . Its charge distribution was calculated within a standard quantum-chemical BKO procedure based on a semiempirical PM3 scheme.² The total solvation energy calculated by the BKO theory was -241 kJ mol^{-1} . The radius for the nonlocal calculation was calibrated to produce the same value, the result being $a_0 = 2.35 \text{ \AA}$. The corresponding inertialless solvation energy for this radius is -131 kJ mol^{-1} , differing from the BKO value of -102 kJ mol^{-1} .

The results from the local BKO and FRCM theories and from nonlocal theory with various values of the quantity τ_λ (2.18) are presented in Figure 2. There is again no significant difference between the local curves. The curve corresponding to the Born solvation energy is also given and is shown to be relatively close to the local curves. However, we see a clear difference in the TCF curves of the local and nonlocal theories. Accounting for solvent structure enables the nonlocal theory to significantly smooth the oscillations seen in the local BKO theory. This indicates its importance in theoretically describing the shape of the TCF function in the intermediate-time region, since no oscillations are usually observed experimentally.^{5,34} Note also that when we consider the various nonlocal curves corresponding to different values of τ_λ (see eq 3.1), we find a natural progression leading from the local BKO results with strong oscillations to the pure ($\lambda(\omega) = \lambda$) nonlocal results with almost no oscillations. This observation is not difficult to explain: for small values of τ_λ the transition in $\lambda(\omega)$ from λ to 0 takes place at very high frequencies, away from region where $\epsilon(\omega)$ has a significant value, and so the solvent dynamics essentially behaves as in the pure nonlocal case. As τ_λ increases, the transition in $\lambda(\omega)$ starts to touch the region of the peaks in $\epsilon(\omega)$ and so part of response function $E(\omega)$ starts to take on a local character. When τ_λ is large enough, the nonlocal character of the system is lost in the intermediate-time region and the TCF behaves as a local-theory function, with corresponding strong oscillations.

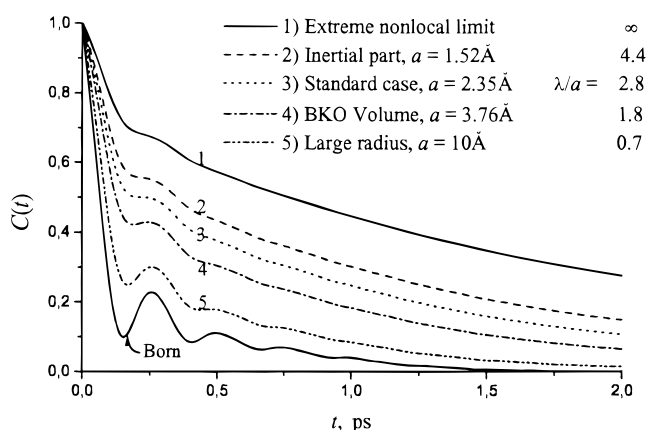


Figure 3. Time correlation functions for a benzophenone anion in acetonitrile, calculated using nonlocal theory. Calculations are made using various estimates of the cavity radius a (see text) with fixed correlation length λ ; i.e., the nonlocality ratio λ/a is systematically varied. The curve for $\lambda/a \rightarrow \infty$ is calculated from eq 4.6. The limiting Born curve ($\lambda/a = 0$) is also shown for comparison.

Another distinction between the local and nonlocal theories is represented by the long-time asymptotic tails of the TCFs. In this region, corresponding to the low-frequency limit $\omega \rightarrow 0$ in the frequency domain, the correlation length (3.1) attains its constant asymptotic value $\lambda(\omega) = \lambda$ and the TCF behavior is completely determined by the ratio λ/a , characterizing the size difference between the solvent and solute particles. The difference is well illustrated in Figure 2, where, for the same value for λ/a , the TCF asymptote becomes independent of τ_λ , the quantity switching $\lambda(\omega)$ from λ to 0. On the other hand, in the Born approximation, the TCF is independent of the cavity radius. We can see from a comparison of the local BKO and Born curves in Figure 2 that the spherical cavity model works sufficiently well for the present case of a multimode $\epsilon(\omega)$ (contrary to the single-mode Debye case, where the effect of the cavity shape is important). This leads us to believe that the same spherical approximation invoked in our nonlocal calculations is more or less reliable.

We study the effect of changing the ratio λ/a by applying different definitions of the ion radius. If we calibrate a using the inertial solvation energy, calibrating eq 2.18 for $\omega = 0$ to $U_s - U_\infty$ from the BKO calculations, then we obtain the smaller value $a_{in} = 1.52 \text{ \AA}$. If on the other hand we define radius a such that the spherical volume in the nonlocal model equals the molecular volume of the complex cavity used in the BKO calculations ($V = 223 \text{ \AA}^3$), then we arrive at a larger value, $a_V = 3.76 \text{ \AA}$. The corresponding TCF curves are compared in Figure 3 for purely nonlocal calculations ($\tau_\lambda = 0$). We see a clear gradation from a curve with minor oscillations to the local Born curve with noticeable oscillations. The gradual approach to the local curve is seen in both the asymptote for larger t and in the increasing amplitude in the oscillations. A curve for $a = 10 \text{ \AA}$ is also given in Figure 3 to confirm this tendency, which shows that the contribution of the small-time resonance mode is maximal in the limiting local case and falls as the degree of nonlocality is increased. This tendency may be expressed quantitatively by fitting the TCF curve to a sum of two exponential functions:

$$C(t) = w_1 e^{-t/\tau_1} + w_2 e^{-t/\tau_2} \quad (4.2)$$

(Three exponential functions may possibly be even more accurate, but two are sufficient for the present argument.) This type of model will, of course, average out the oscillations.

TABLE 1: Coefficients for a Two-Exponential Fit to the Time Correlation Functions (Including the Solvent Resonance Region) from Nonlocal Theory for Various Values of λ/a^a

λ/a	w_1	τ_1 (ps)	w_2	τ_2 (ps)
0 (Born)	0.9	0.07	0.1	0.8
0.7	0.75	0.09	0.25	0.9
1.8	0.55	0.10	0.45	1.12
2.8	0.48	0.11	0.52	1.32
4.4	0.42	0.11	0.58	1.52
∞	0.31	0.16	0.67	2.34

^a $C(t) = w_1 \exp(-t/\tau_1) + w_2 \exp(-t/\tau_2)$. The calculations for the limit $\lambda/a \rightarrow \infty$ are made using eq 4.6. The limiting local born result is also shown for comparison. The time constants may be compared with the longitudinal and Debye time constants for acetonitrile: $\tau_L = 0.169$ ps and $\tau_D = 3.37$ ps, respectively.

Results are presented in Table 1. Here we distinctly see that as the nonlocal ratio λ/a increases, the weight of the long-time mode increases. The time constant of the short-time mode remains mostly unchanged over all values of λ/a ; it is completely dominant when $\lambda/a = 0$ but drops in significance as λ/a increases. The time constant of the long-time mode, on the contrary, increases with increasing λ/a , reaching a limiting value when $\lambda/a \rightarrow \infty$ (see section 4.3 below).

4.3. Analysis of the Low-Frequency (Long-Time) Limit of the Nonlocal Theory. The extreme nonlocal limit may be analyzed more carefully by studying eq 2.18 analytically. Although ultimately as $\lambda/a \rightarrow \infty$, the solvation energy will remain unchanged kinetically at the value of the inertialless solvation energy,¹⁹ given by eq 2.17, we are nevertheless able to describe separately the dynamics as this limit is being reached. Here we are mainly interested in the long-time tail, i.e., low frequencies; therefore we write in eq 2.18 $\lambda(\omega) = \lambda$. Using the limit $\coth x \approx 1/x$ for small x , we find that the solvation energy reduces in the extreme nonlocal limit to

$$\lim_{\lambda/a \rightarrow \infty} E(\omega) = -\frac{Q^2}{2a} \left(\frac{1}{\epsilon_\infty} - \frac{1}{\epsilon(\omega)} \right) \frac{1}{1 + \lambda/a \sqrt{\epsilon_\infty/\epsilon(\omega)}} \quad (4.3)$$

It is expedient to write this expression in the form

$$E(\omega) = E_0 \Delta(\omega) \quad (4.4)$$

where $E_0 = E(\omega = 0)$ and $\Delta(\omega = 0) = 1$. Although in the nonlocal limit $\lambda/a \rightarrow \infty$, E_0 falls to zero, the dynamical function $\Delta(\omega)$, which is given by the formula

$$\Delta(\omega) = \left(\frac{1/\epsilon_\infty - 1/\epsilon(\omega)}{1/\epsilon_\infty - 1/\epsilon_0} \right) \left(\frac{1 + \lambda/a \sqrt{\epsilon_\infty/\epsilon_0}}{1 + \lambda/a \sqrt{\epsilon_\infty/\epsilon(\omega)}} \right) \quad (4.5)$$

does not disappear. In the extreme nonlocal limit the ratio λ/a cancels out and $\Delta(\omega)$ may be written as

$$\Delta(\omega) = \frac{\epsilon(\omega) - \epsilon_\infty}{\epsilon_0 - \epsilon_\infty} \sqrt{\frac{\epsilon_0}{\epsilon(\omega)}} \quad (4.6)$$

The corresponding TCF is shown in Figure 3 and its two-exponent fit given in Table 1. The long-time tail may be studied further by inserting a Debye function with relaxation time τ_D for $\epsilon(\omega)$ (valid for small ω) into eq 4.5 and finding the Taylor expansion:

$$\Delta(\omega) = 1 + \frac{i\omega\tau_L}{2} \left(1 + \frac{1 + \lambda/a \sqrt{\epsilon_0/\epsilon_\infty}}{1 + \lambda/a \sqrt{\epsilon_\infty/\epsilon_0}} \right) + O[\omega^2] \quad (4.7)$$

where τ_L is the longitudinal time constant $\tau_L = \tau_D \epsilon_0/\epsilon_\infty$. Formula 4.7 suggests that, within a first-order analysis, the nonlocal dynamical function $\Delta(\omega)$ can be described approximately by two Debye functions of equal weighting:

$$\Delta(\omega) = \frac{0.5}{1 - i\omega\tau_L} + \frac{0.5}{1 - i\omega\tau_{nl}} + O[\omega^2] \quad (4.8)$$

and consequently the TCF will be $C(t) \approx 0.5 \exp(-t/\tau_L) + 0.5 \exp(-t/\tau_{nl})$. Here τ_{nl} is the larger "nonlocal" time constant

$$\tau_{nl} = \tau_L \frac{1 + \lambda/a \sqrt{\epsilon_0/\epsilon_\infty}}{1 + \lambda/a \sqrt{\epsilon_\infty/\epsilon_0}} \quad (4.9)$$

It follows that the slow time constant seen for the extreme nonlocal limit in Figure 3 and Table 1 is, again to a first-order approximation, none other than the Debye constant:

$$\lim_{\lambda/a \rightarrow \infty} \tau_{nl} = \tau_D \quad (4.10)$$

The difference between the values of the weights and time constants of the two modes shown here from those given in Table 1 is presumably due to the higher order terms and the fact that the figures in the table include the resonance region, unlike the asymptotic values given here. To follow the transition to the local limit in a similar way, the Taylor expansion must be drawn from the full expression eq 2.18. This will clearly yield the result $\tau_{nl} = \tau_L$ for the long-time decay kinetics when $\lambda/a \rightarrow 0$; incidently, formula eq 4.9 also reproduces this result. That is, the dynamics for our nonlocal spherical model reduces to the single-exponential dynamics of the simplest dynamical continuum theory. The nature of the nonlocal time constant τ_{nl} would appear to suggest that the Lorentzian nonlocal dielectric function used here (eqs 2.14 and 2.16), is consistent with the Onsager "inverted snowball" picture,³⁵ describing orientational relaxation only, in which solvation relaxation far from the ion ("a" large) is characterized by τ_L and close to ion ("a" small) by τ_D . It seems reasonable to expect that the more complex kinetics found by considering the relaxation of solvation shells independently¹² could be obtained in continuum theory by using more realistic models of the nonlocal dielectric function.²⁵

5. Discussion

Simple spherical continuum models predict monoexponential TCF kinetics when the solvent model contains a single relaxation mode (a Debye solvent).^{5,14} This deficiency is removed by taking into account nonspherical solute shapes; with such a modification polyexponential kinetics may be seen even for a Debye solvent.^{1,2,3,7} On the other hand, this obvious drawback of Born-like solvation theories disappears when real multimode solvent models are considered; in this case, which is intrinsically polyexponential, local continuum calculations with both spherical and molecular-shaped solute models predict very similar results. They all reproduce satisfactorily experimental polyexponential TCF kinetic curves provided accurate dielectric function based on experimental measurements are introduced as input data^{1,3,5} (see also the present work).

We mention here that although for this paper we calculated the time correlation function numerically, we did in fact also

attempt approximating the calculated response function $E(\omega)$ with several analytical functions (cf. ref 29) for which inverse Fourier transforms are known. The accuracy of this procedure was found to be lower than the numerical inverse Fourier transform of eqs 2.9 and 2.10, in the sense that the long-time asymptote in the TCF for $t > 1$ ps significantly deviated from the experimental curve. However, the analytical models could be useful for establishing the limiting behavior for $t \rightarrow 0$, which is reported to have a Gaussian shape.^{33,36,37} The $E(\omega)$ curves were found to be best modeled by a combination of Gaussian functions, whose imaginary parts produced either a broad peak ($\omega \exp[-\tau^2(\omega^2 - \bar{\omega}^2)]$) or a narrow peak ($\exp[-\tau^2(\omega - \bar{\omega})^2] - \exp[-\tau^2(\omega + \bar{\omega})^2]$) (the latter in the resonance region) and modified Debye functions of the type $1/((1 - i\omega\tau)(1 - i\omega\tau_\infty))$, $\tau_\infty \ll \tau$ (in the orientational region). Each of these functions, whose inverse Fourier transform and hence TCF can be calculated analytically, has the correct asymptotic behavior of $1/\omega^2$ as $\omega \rightarrow \infty$, which corresponds to short-time Gaussian behavior in the TCF: $C(t) = 1 - bt^2$, $t \rightarrow 0$ for some constant b . Finally, we note also in this context that the narrow-peak Gaussian function generates an oscillating TCF (the other two are monotonic). Therefore the fact, described below, that the local BKO and FRCM theories produce an oscillating TCF suggests that this particular peak is exaggerated by these theories. However, for the sake of an accurate description of the TCF for the asymptote at $t > 1$ ps, we have reported here only the results from numerical transformations.

The situation looks more complicated when a nonlocal solvation theory is invoked. For Debye solvents, a nonlocal approach always yields polyexponential kinetics, even with spherical solute models (which in fact are the only models tractable in a nonlocal theory). This is seen from the results of the present work as well as from earlier MSA treatments,⁸⁻¹⁰ which are in fact a special case of nonlocal theory. When working with real multimode dielectric functions, a significant discrepancy between local and nonlocal treatments still remains. First, the nonlocal approach is found to smoothe oscillations in the TCF curve in the intermediate time interval ($0.1 \text{ ps} < t < 1 \text{ ps}$). Such oscillations, not characteristic of experiments, appear in all local calculations when a resonance mode is included in the dielectric function, no matter how sophisticated the treatment of the solute shape. Second, local and nonlocal theories differ significantly in describing the long-time exponential tails of the TCF curves. This observation, made in the present work, can be understood in terms of the basic nonlocal parameter λ/a , the ratio of the average sizes of solvent and solute particles ($\lambda/a = 0$ in the local theories). However, our observations are made only for the limited case of an ionic solute, for which experimental tests are mostly unavailable at the present time. It is likely that solvent relaxation in the vicinity of dipolar solute particles will not be so remarkably dependent on the solute size. We are presently unable to judge the real importance of this size effect, but the ambiguity could be resolved by further theoretical studies of nonlocal dynamical effects for dipolar solutes. Systematic experimental measurements of TCFs for solutes of varying size in the same solvent would also be relevant for this purpose.

Acknowledgment. The authors would like to thank Prof. M. Maroncelli for kindly providing the $\epsilon(\omega)$ resonance data for acetonitrile and the experimental data for the TCF of coumarin-153 in acetonitrile. The research was made possible in part by

Award No. RC1-202 of the U.S. Civilian Research and Development Foundation for the Independent States of the Former Soviet Union (CRDF) and by the International Association for the Promotion of Cooperation with Scientists from the New Independent States of the Former Soviet Union (project INTAS-RFBR 95-0182). M.V.B. and M.V.V. also acknowledge financial support from the Russian Foundation for Basic Research (grant No. 96-03-32544 and No. 96-15-97465).

Appendix: Approximate FRCM Equations with Complex-Valued $\epsilon(\omega)$

We consider two cavities bounded by the surfaces S_1 (inner surface) and S_2 (outer surface). The dielectric function is

$$\epsilon(\omega) = \begin{cases} 1 & \text{(inside } S_1) \\ \epsilon_\infty & \text{(between } S_1 \text{ and } S_2) \\ \epsilon_1(\omega) + i\epsilon_2(\omega) & \text{(outside } S_2) \end{cases} \quad (\text{A.1})$$

We may define a series of surface integral operators \hat{S}_{ij} ($i, j = 1, 2$), acting on an arbitrary function $f(r)$, by

$$\hat{S}_{ij}f(r) = \int_{S_j} d^2r' a(r, r') f(r') \quad r \in S_i \quad (\text{A.2})$$

where

$$a(r, r') = \frac{\partial}{\partial n(r)} \frac{1}{|r - r'|} \quad (\text{A.3})$$

We also define the operator \hat{V}

$$\hat{V}\rho(r) = \int d^3r' a(r, r')\rho(r') \quad (\text{A.4})$$

Here $\rho(r)$ is the solute charge density, contained in the first cavity. If we then label the inner surface charge density as σ_∞ and the outer as $\sigma = \sigma_1 + i\sigma_2$, we find that under the approximation described in section 2.2 (neglecting the influence of the outer surface charge on the inner), the FRCM equations¹⁷ reduce to

$$\sigma_\infty = \frac{1}{4\pi} \left(1 - \frac{1}{\epsilon_\infty} \right) [\hat{V}\rho + \hat{S}_{11}\sigma_\infty + 2\pi\sigma_\infty] \quad r \ll S_1 \quad (\text{A.5})$$

and

$$\sigma = \frac{1}{4\pi} \left(1 - \frac{\epsilon_\infty}{\epsilon(\omega)} \right) [\hat{V}\rho + \hat{S}_{21}\sigma_\infty + \hat{S}_{22}\sigma + 2\pi\sigma] \quad r \in S_2 \quad (\text{A.6})$$

By separating the real and imaginary parts of the latter equation, we obtain two simultaneous equations for the real and imaginary parts of σ for each value of ω :

$$\sigma_1 = \kappa_1 [(\hat{V}\rho(r) + \hat{S}_{21}\sigma_\infty) + (\hat{S}_{22} + 2\pi)\sigma_1] - \kappa_2 (\hat{S}_{22} + 2\pi)\sigma_2 \quad (\text{A.7})$$

$$\sigma_2 = \kappa_2 [(\hat{V}\rho(r) + \hat{S}_{21}\sigma_\infty) + (\hat{S}_{22} + 2\pi)\sigma_1] - \kappa_1 (\hat{S}_{22} + 2\pi)\sigma_2 \quad (\text{A.8})$$

where

$$\kappa_1 = \frac{1}{4\pi} \left(1 - \frac{\epsilon_\infty \epsilon_1}{(\epsilon_1)^2 + (\epsilon_2)^2} \right) \quad (\text{A.9})$$

$$\kappa_2 = \frac{1}{4\pi} \left(\frac{\epsilon_\infty \epsilon_2}{(\epsilon_1)^2 + (\epsilon_2)^2} \right)$$

References and Notes

- (1) Hsu, C.-P.; Song, X.; Marcus, R. *J. Phys. Chem. B* **1997**, *101*, 2546.
- (2) Basilevsky, M.; Parsons, D.; Vener, M. *J. Chem. Phys.* **1998**, *108*, 1103.
- (3) Song, X.; Chandler, D. *J. Chem. Phys.* **1998**, *108*, 2594.
- (4) Ovchinnikov, A. A.; Ovchinnikova, M. Y. *Zh. Eksp. Teor. Fiz.* **1969**, *62*, 2583, in Russian.
- (5) Horng, M.; Gardecki, J.; Papazyan, A.; Maroncelli, M. *J. Phys. Chem.* **1995**, *99*, 17311.
- (6) van der Zwan, G.; Hynes, J. T. *J. Phys. Chem.* **1985**, *89*, 4181.
- (7) Bagchi, B.; Castner, E. W.; Fleming, G. R. *J. Mol. Struct.* **1989**, *194*, 171.
- (8) Wolynes, P. G. *J. Chem. Phys.* **1987**, *86*, 5133.
- (9) Rips, I.; Clafter, J.; Jortner, J. *J. Chem. Phys.* **1988**, *88*, 3246.
- (10) Rips, I.; Clafter, J.; Jortner, J. *J. Chem. Phys.* **1988**, *89*, 4288.
- (11) Bagchi, B.; Chandra, A. *Adv. Chem. Phys.* **1991**, *80*, 1.
- (12) Rips, I. In *Ultrafast Reaction Dynamics and Solvent Effects*; Gaudel, Y., Rosky, P. J., Eds.; AIP Press: New York, 1994; pp 334–344.
- (13) Kornyshev, A.; Kuznetsov, A.; Phelps, D.; Weaver, M. *J. Chem. Phys.* **1989**, *91*, 7159.
- (14) Maroncelli, M. *J. Mol. Liq.* **1993**, *57*, 1.
- (15) Song, X.; Marcus, R. *J. Chem. Phys.* **1993**, *99*, 7768.
- (16) Boettcher, C.; Bordewijk, P. *Theory of electric polarization*, 2nd ed.; Elsevier: Amsterdam, 1978; Vol. 2.
- (17) Basilevsky, M.; Rostov, I.; Newton, M. *Chem. Phys.* **1998**, *232*, 189.
- (18) Basilevsky, M.; Parsons, D. *J. Chem. Phys.* **1996**, *105*, 9734.
- (19) Basilevsky, M.; Parsons, D. *J. Chem. Phys.* **1998**, *108*, 9107.
- (20) Tomasi, J.; Persico, M. *Chem. Rev.* **1994**, *94*, 2027.
- (21) Basilevsky, M. V.; Chudinov, G. E. *Chem. Phys.* **1991**, *157*, 345.
- (22) Basilevsky, M. V.; Chudinov, G. E.; Newton, M. D. *Chem. Phys.* **1994**, *179*, 263.
- (23) Newton, M.; Basilevsky, M.; Rostov, I. *Chem. Phys.* **1998**, *232*, 201.
- (24) Basilevsky, M.; Chudinov, G.; Rostov, I.; Liu, Y.-P.; Newton, M. *J. Mol. Struct. (THEOCHEM)* **1996**, *371*, 191.
- (25) Basilevsky, M. and Parsons, D. *J. Chem. Phys.* **1998**, *108*, 9114.
- (26) Firman, P.; Marchetti, A.; Xu, M.; Eyring, E.; Petrucci, S. *J. Phys. Chem.* **1991**, *95*, 7055.
- (27) Arnold, K.; Yarwood, J.; Price, A. *Mol. Phys.* **1983**, *48*, 451.
- (28) Song, X.; Chandler, D.; Marcus, R. *J. Phys. Chem.* **1996**, *100*, 11954.
- (29) Basilevsky, M.; Chudinov, G. *J. Chem. Phys.* **1995**, *103*, 1470.
- (30) Moyland, C. *J. Phys. Chem.* **1994**, *98*, 13513.
- (31) Baumann, W.; Nagy, Z. *Pure Appl. Chem.* **1993**, *65*, 1729.
- (32) McCarthy, P.; Blanchard, G. *J. Phys. Chem.* **1993**, *97*, 12205.
- (33) Carter, E.; Hynes, J. *J. Chem. Phys.* **1991**, *94*, 5961.
- (34) Maroncelli, M.; MacInnis, J.; Fleming, G. *Science* **1989**, *243*, 1674.
- (35) Onsager, L. *Can. J. Chem.* **1977**, *55*, 1819.
- (36) Bruehl, M.; Hynes, J. *J. Phys. Chem.* **1992**, *96*, 4068.
- (37) Smith, B.; Staib, A.; Hynes, J. *Chem. Phys.* **1993**, *176*, 521.